Geophys. J. Int. (2004) **158,** 98–108 doi: 10.1111/j.1365-246X.2004.02262.x

Earthquakes as three stage processes

F. Mulargia, S. Castellaro and M. Ciccotti

Dipartimento di Fisica, Settore di Geofisica, University of Bologna, Italy. E-mail: mulargia@ibogfs.df.unibo.it

Accepted 2004 February 6. Received 2004 February 6; in original form 2003 January 20

SUMMARY

Relying on basic physics, laboratory and field evidence, and accounting for the different timescales involved, we derive an approximate energy function for earthquakes. The fracture term is disregarded because virtually all earthquakes occur on pre-existing faults and because fault gouge has a very low fracture energy. Disregarding also the gravitational term, the importance of which depends on the type of seismic focal mechanism, yields that the energy function has only thermal and radiative terms. The self-similarity ranges in the bulk rocks and gouge suggest taking the basic element as two cubes of 10 m side, with in common one face, over which slip occurs. An earthquake is a cascade of such slip processes on a series of neighbouring elements and the volume involved can be self-similarly defined as the two megacubes embedding the set of elements participating in the slip. Dimensional analysis suggests that the slip process is composed of three stages. The first stage consists of a stick-slip episode with an average velocity $v \sim 10^{-1}$ m s^{-1} over a time $t \sim 10^{-2}$ s. In this first stage, stage I, virtually all energy is converted into heat, with a temperature increase of the order of 10^2 K on the sliding surface. The second stage, stage II, in which the occurrence of further slip episodes is hardly relevant, consists of the propagation of the thermal wave generated in stage I to the whole shear zone, with a characteristic time of the order of 10^2 s. In light of the comparatively low permeability of fault gouge with respect to heat diffusivity, this temperature increase induces a pore fluid pressure increase. When the transition from hydrostatic to lithostatic pressure is completed over the whole shear zone, a third stage, stage III, is entered, in which, provided that the pressurization is maintained, virtually frictionless high-velocity slip occurs, converting all the available energy into elastic radiation. The duration of this purely radiative stage, the amount of slip and the size of the earthquake depend on the number of elements cooperatively participating in the cascade slip, which is ruled, just as in the usual single-stage cellular automata models, by the correlation length over which the strain level is near the rupture threshold. At odds with the classical single-stage cellular automata, the model does not require the introduction of strong jumps in stress to be ignited and appears thus also capable of explaining the Coulomb failure stress quandary of very small triggering stresses, with the ignition of large events requiring excess stresses of just 10^{-2} to 10^{-3} MPa. The global seismic efficiency, under the assumption that granular effects and viscous resistance are disregarded, is ~ 1. Assuming then statistical self-similarity on the fault plane for the patches that slip cooperatively and approximating their pattern as a Sierpinski carpet, yields partial and approximately constant stress drop values independent of event size. These emerge from the fractal nature of the slip surface interpreted according to the seismological assumption of constant homogeneous slip on the Euclidean rectangular plane fault, which embeds the slipping patches.

Key words: Coulomb failure stress, earthquake source mechanism, earthquake triggering, fluid pressure, ignition slip, self-similarity.

1 INTRODUCTION

In physics, the common approach to describe a phenomenon is to write its energy equation. Writing this equation for an earthquake is difficult for both its direct inaccessibility and its complex phenomenology. Earthquake models do exist that are satisfactory for what regards the far-field elastic radiation (Ben-Menahem 1995), but these are incapable of describing event recurrence, so that the

prediction of single earthquakes is an untenable goal (Geller *et al.* 1997a,b). In addition to this, even the basic physical phenomenon, which is the stick-slip of two crustal rock blocks, appears to be incompatible with the heat flow measurements on active fault systems. In fact, according to current earthquake models, very large amounts of frictional heat should be generated by seismic fault slip, but the heat flow measurements along the San Andreas and other faults have consistently reported only modest heat values (Brune *et al.* 1969; Lachenbruch & Sass 1980), leading to what is termed the fault strength paradox (*cf.* Ben-Zion 2001).

Here, relying on simple dimensional analysis and accounting for the very different timescales involved, we attempt first of all to write an approximate earthquake energy function. Secondly, based on this energy function, we cast a three-stage self-similar earthquake model able to accommodate the above as well as the other basic phenomenology.

2 EARTHQUAKE BASIC PHENOMENOLOGY

Earthquake phenomenology is complex. Its basic features are:

(i) Earthquakes are rare events.

(ii) Earthquakes are clustered in both space and time (Kagan & Jackson 1991).

(iii) Earthquakes are rupture and slip events, which occur mostly on pre-existing faults.

(iv) Earthquakes have an approximately constant stress drop, which is considerably smaller than ambient stress (Abercrombie & Leary 1993).

(v) The external forcing function, that is tectonic strain, is small and constant, inducing extremely low strain rates.

(vi) Faults are rough surfaces, with power-law scaling suggestive of fractal geometry, albeit with fractal dimension close to 2 (the Euclidean plane) in the range 10^2 to 10^4 m (Okubo & Aki 1987).

(vii) The spatial distribution of earthquake hypocentres and laboratory acoustic emission locations are power law in both space and time (Kagan & Knopoff 1980; Hirata *et al.* 1987).

(viii) Earthquakes are power-law distributed in size in terms of a variable 10^m, where m is magnitude (Gutenberg–Richter law).

(ix) Earthquakes have aftershock sequences that decay as a power law in time (Omori law).

The latter features share a generalized power-law behaviour, which in statistical mechanical terms is equivalent to the intrinsic self-similarity of the process (*cf.* Bak & Tang 1989; for a comprehensive view see Mulargia & Geller 2003).

3 THE SELF-SIMILAR SOURCE

Let us consider a portion of crust containing a fault patch that is large enough to disregard grain size. Because virtually all earthquakes occur on pre-existing faults, the grain size will be that of the fabric of fault gouge, which is the crushed and reworked incoherent material that surrounds the faults. This fabric has a power-law distribution with no apparent upper cut-off for lengths up to the order of a few 10^{-3} m (Sammis *et al.* 1986). Consistent with this, we take the thickness of the shear zone of the order of a few 10^{-2} m. We aim at a self-similar description over a finite range with the upper cut-off given by crustal thickness, which means that our self-similar description will include all but the largest earthquakes. As a lower cut-off we take a geometrical entity of linear dimension of $\sim$ 10 m,

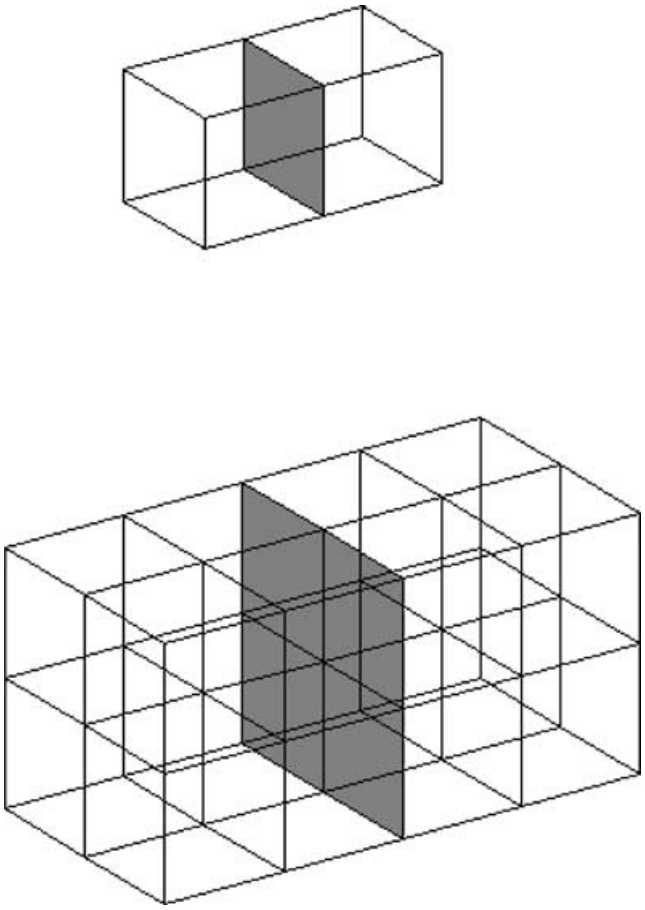

Figure 1. The self-similarity relation, with slip occurring at the contact face. Strain remains constant. The linear dimension of each cell is $\sim$ 10 m.

above which the scale invariance of crustal rocks appears reasonably well satisfied (*cf.* Ouillon *et al.* 1996). We will therefore define our basic element as two cubes of 10 m side, with the face in common representing the fault patch over which slip occurs (see Fig. 1). Self-similarity will be accommodated by letting this geometry repeat identically up to a 10 km side, with the obvious constraints imposed by the fact that self-similarity occurs on a finite range of approximately 3.5 decades, the details of which are discussed later in the paper. In the following, we first describe the process relative to the basic element.

4 EARTHQUAKE ENERGY FUNCTION

Disregarding the gravitational term, the importance of which varies depending on individual fault mechanism and geometry, four terms can be considered in the earthquake energy function Ψ:

$$\Psi = E_E + E_F + E_R + E_T, \tag{1}$$

where E_E is the available elastic energy, E_F is the fracture energy, E_R is the radiated energy and E_T is the thermal energy.

4.1 The elastic energy

Earthquakes are produced by shear deviatoric stresses. The most simple case restricts the discourse to a single shear strain component ϵ and from the theory of elasticity, the elastic energy stored in the

volume V is

$$E_E = \int_V \frac{1}{2}\mu\epsilon^2\, dV, \tag{2}$$

where μ is modulus of rigidity. The largest coseismic crustal strains are of the order of 10^{-3}, so that, because in the Earth's crust $\mu \sim 10^{10}$ Pa, the maximum available deviatoric elastic energy per unit volume is approximately 10^4 J m^{-3}.

In order to proceed, we need to introduce a seismic source model. The standard seismic source model is a plane dislocation (Brune 1968) of linear dimension r and area A proportional to r^2. We approximate the crust as a 3-D lattice composed of our basic elements of side r and apply the standard seismic model to the sliding patch of a basic element, which is subject on the sliding plane to a shear stress σ, assumed constant. Let us also assume that the friction stress is a material constant equal to σ_f.

Consider a slip s on the patch, where s is a small fraction $\eta \ll 1$ of r, $\eta \sim 10^{-3}$. Consistent with the assumed value for r (10 m)

$$s = \eta r \simeq 10^{-2}\,\text{m}. \tag{3}$$

According to Volterra's theorem, the work done by this slip is (Landau & Lifshitz 1970; Ben-Menahem & Singh 1981)

$$\Delta W = \langle\sigma\rangle s A = E_E, \tag{4}$$

where $\langle\sigma\rangle$ is the average stress during the slip. This slip involves contributions in the radiated, fracture and thermal energies. Let us analyse how the work is partitioned among them by estimating the different contributions produced by a slip s.

4.2 The radiated energy

The radiated energy E_R can be directly estimated from the recorded seismic waves by considering that the ground displacement x at a given point reached at the time t by a seismic wave of amplitude a and period T is (Gutenberg & Richter 1956)

$$x = a\cos\left(\frac{2\pi t}{T}\right). \tag{5}$$

The average kinetic energy E_{kin} imposed by the passing wave in a medium of density ρ per unit volume is then (*cf.* Kasahara 1981)

$$\begin{aligned} E_{\text{kin}} &= \frac{\rho}{2}\dot{x}^2 = \frac{\rho}{2T}\int_0^T \dot{x}^2 dt \\ &= \frac{\rho}{2T}\left(\frac{2\pi a}{T}\right)^2 \int_0^T \sin^2\left(\frac{2\pi t}{T}\right) dt = \rho\pi^2\left(\frac{a}{T}\right)^2 \end{aligned} \tag{6}$$

and the total energy is twice as much because it includes an identical amount of potential energy (ibid.). Integration over the boundary surface of a volume containing the source then gives the measure of the total energy of the radiated waves. In practice, it is convenient to rely on more readily measured quantities. Considering the slip of the patch as whole, the basic quantity is the scalar seismic moment M,

$$M = \mu s A, \tag{7}$$

in terms of which the total radiated energy can be written as

$$E_R = \Delta W_R = (\langle\sigma\rangle - \sigma_f)\frac{M}{\mu}, \tag{8}$$

where σ_f is the average friction stress. Disregarding the difference between static and dynamic stress, considering the stress values before and after the slip, σ_{init} and σ_{end}, respectively, the above formula can also be written as

$$E_R = (\langle\sigma\rangle - \sigma_{\text{end}})\frac{M}{\mu} = \frac{\Delta\sigma M}{2\mu}, \tag{9}$$

where $\Delta\sigma$ is the stress drop.

4.3 The fracture energy

The estimates of the fracture energy traditionally rely on energy conservation (Griffith 1920). If a new crack is formed or an existing crack propagates, free surfaces are created by the breaking of bonds. It would appear tempting to generalize the Griffith approach, which works reasonably well on homogeneous and isotropic laboratory brittle specimens of simple geometry and with a single crack, to include real systems, which regard a generic material with a population of cracks. Unfortunately, in the general case the simple Griffith picture does not work as a result of the presence of dissipative terms and (at propagation velocities comparable to those of the elastic waves) kinetic effects, which are often more important than the elastic terms themselves (*cf.* Herrmann & Roux 1990). In addition to this, seismic faults occur in fault gouge, which has mechanical features very different than those of bulk rock (*cf.* Mora *et al.* 2000).

As a consequence, the estimates of fracture energy E_F made using the approximation of a single propagating mode III crack in an elastic brittle continuum (Kostrov 1966; Eshelby 1969; Dahlen 1977; Freund 1998), which are popular in the seismological approach to earthquake physics, must be regarded as restrictive. Physically, it appears more appropriate to rely directly on experimental fracture energy data relative to sliding experiments with realistic fault gouge. The latter indicate a fracture energy 3 to 4 orders of magnitude smaller than the total energy (Yoshioka 1986), so that, because we are not considering the case of fresh faulting, fracture energy can be comfortably disregarded.

4.4 The thermal energy

For energy balance we have

$$\Delta W_T = \sigma_f s A = E_T, \tag{10}$$

where the average friction stress σ_f is equal to

$$\sigma_f = \sigma_n\phi, \tag{11}$$

with σ_n indicating the stress normal to the fault surface and ϕ the coefficient of friction, which, under static and kinetic configuration for a variety of rocks at seismogenic depth conditions, falls in the range $\sim$ 0.6–0.9 according to both laboratory (Byerlee 1978) and borehole *in situ* stress measurements (McGarr & Gay 1978; Brudy *et al.* 1997). The values of σ_n in the crust can be taken to be of the order of 10^8 Pa (ibid.).

The rate of heat q generated per unit area by fault slip can be roughly calculated by using the equation for a plane surface in an infinite medium

$$q = \sigma_n\phi v, \tag{12}$$

where v is the slip velocity and σ_n is the stress normal to the fault plane. If pore fluids are present, as it is the general case of water in fault gouge (Morrow *et al.* 1984), eq. (12) reads as

$$q = (\sigma_n - P_p)\phi v, \tag{13}$$

where P_p is the fluid pore pressure, which is hydrostatic at equilibrium.

Assuming that heat generation starts at time $t = 0$ as a step function with a constant heat flux q, the temperature rise ΔT at a distance x from the emitting plane surface after a time t is, calling C the specific heat and K the thermal diffusivity (Carslaw & Jaeger 1986),

$$\Delta T = \frac{q}{\rho C}\left(\sqrt{\frac{t}{\pi K}}\right) e^{-\frac{x^2}{4Kt}} - \left[\left(\frac{q}{\rho C}\right)\left(\frac{|x|}{2K}\right)\mathrm{erfc}\left(\frac{|x|}{2\sqrt{Kt}}\right)\right], \tag{14}$$

which, close to the fault surface, i.e. when $|x| < \sqrt{Kt}$, can be approximated as (Sibson 1975)

$$\Delta T = \frac{q}{k}\sqrt{\frac{Ks}{\pi v}}, \tag{15}$$

where k is the thermal conductivity and $s = vt$ is the displacement at time t. Combining the last equation with eq. (13)

$$\Delta T = \frac{\phi(\sigma_n - P_p)}{k}\sqrt{\frac{Ksv}{\pi}}. \tag{16}$$

Based on laboratory evidence, reasonable values of the parameters involved are $K = 10^{-6}$ m^2 s^{-1}, $k = 2$ J/(m s$^\circ C$) (Clark 1966). This yields that temperatures should raise locally above 10^3 K for velocities and displacements typical of seismic events because, as indicated by the size of the shear zone, sliding seems to be concentrated in a zone of a few 10^{-2} m. However, the presence of melting products like pseudotachylites appears to be rare (Sibson 1975) and therefore some mechanism capable of substantially reducing friction and frictional heating must exist. Note that melting itself might in principle reduce friction (Kanamori & Heaton 2000), but there are basic difficulties for this (see discussion in Section 5.4).

5 EARTHQUAKES AS A THREE-STAGE PROCESS

Let us relax the assumption shared by all the proposed mechanisms of friction reduction that slip occurs at a single timescale (*cf*. Ben-Zion 2001) and consider a first stage of high friction stick-slip similar to that encountered in the laboratory.

5.1 Stage I

The process starts when strain build-up induces on the fault patch a stress σ such that

$$\sigma > \sigma_f. \tag{17}$$

Sliding occurs, doing work

$$\Delta W = \Delta W_R + \Delta W_T, \tag{18}$$

because, as we have seen, the fracture energy can be disregarded.

This work is also equal to

$$\Delta W = \int_\Sigma \sigma\, Ads, \tag{19}$$

where Σ is the propagation domain in which

$$\sigma > \sigma_f, \tag{20}$$

because slip stops when the elastic force is less than the friction force.

According to eqs (10)–(13) the thermal work is

$$\Delta W_T = \int_\Sigma (\sigma_n - P_p)\phi\, Ads, \tag{21}$$

which can be approximated as

$$(\sigma_n - P_p)\phi s A. \tag{22}$$

In agreement with laboratory phenomenology, slip occurs in stick-slip episodes, with $\phi \simeq 0.6$–0.9, average velocity values of the order of 10^{-2} m s^{-1}, peak velocity values of the order of 10^{-1} m s^{-1} and a radiated elastic energy that is a fraction of order 10^{-2} of the thermal energy (e.g. Lockner & Okubo 1983), so that

$$\Delta W \simeq \Delta W_T. \tag{23}$$

In other words, virtually all the work done according to eq. (21) is transformed into heat

$$\Delta W_T = \Delta Q = CAw\rho\Delta T \sim Cr^2 w\rho\Delta T, \tag{24}$$

where w the width of the thermal zone, the latter being the volume surrounding the fault plane in which temperature increases. Rewriting eq. (16), slip is accompanied by a temperature ΔT increase of the matter surrounding the slip plane equal to

$$\Delta T \simeq (\sigma_n - P_p)\frac{\phi}{k}\sqrt{\frac{Kv^2 t}{\pi}}, \tag{25}$$

where t is time, which yields that temperatures of the order of 10^2 K are attained by a stick-slip episode with an average $v^2\, t \sim 10^{-4}$ m^2 s^{-1}. Considering laboratory experiments, such an episode is likely to be constituted by a cluster of stick-slip events, with an average velocity $v \sim 10^{-1}$ m s^{-1} over a time of 10^{-2} s, implying a total slip of the order of 10^{-3} m. On the unit patch this corresponds to a strain release of the order of 10^{-4} and, because the maximum accumulated strain is of the order of 10^{-3}, stage I consumes a strain energy $\sim \Delta W_T$, which leaves the total strain energy almost intact (*cf.* eq. 2). The released strain decreases the stress from $\sigma > \sigma_f$ to $\sigma < \sigma_f$, thus stopping the slip.

5.2 Stage II

Stage I has raised the temperature on the friction surfaces within the shear zone to a value of the order of 10^2 K with a slip episode of a duration of 10^{-2} s. The width w over which heat is carried by thermal diffusion is

$$w(t) = 2\sqrt{Kt}, \tag{26}$$

which means that the heat wave will propagate to the whole shear zone, which has a width w of the order of a few 10^{-2} m, in a time of the order of 10^2 s after the slip event. Experimental values for permeability in fault gouge after a sliding of the order of 10^{-3} m are around 10^{-9} Darcy (or $<10^{-21}$ m^2) (Morrow *et al.* 1981, 1984; Zhang & Tullis 1998) and the resulting Darcy diffusivity K_D, of the order of 10^{-8} m^2 s^{-1}, is smaller than thermal diffusivity K (of the order of 10^{-6} m^2 s^{-1}). Therefore, the temperature increase resulting from frictional sliding diffuses faster than the thermally expanded pore fluid and, when it extends to the whole shear zone, it raises the fluid pressure from hydrostatic to lithostatic, decreasing the effective normal stress, and thus (static) friction, towards zero. Because in frictional sliding the largest asperities dominate the process (Scholz 1990), only when the whole shear zone has been pressurized a transition to friction values near zero occurs. Further stick-slip episodes may take place during this stage, but they can reduce the time required to heat the whole shear zone only if their position is such that they generate thermal waves that travel ahead of the original one.

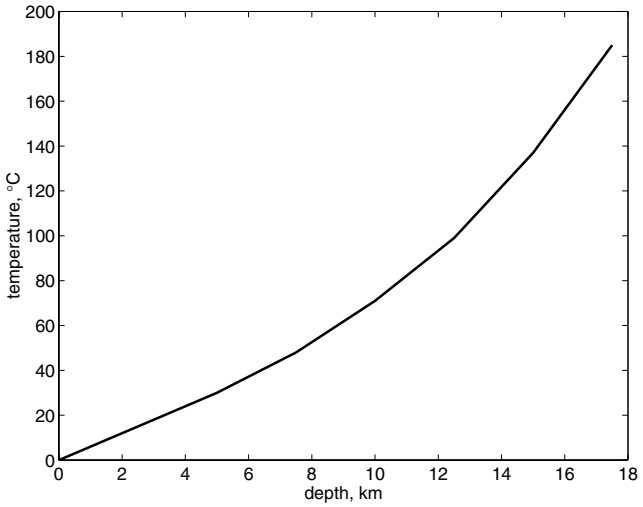

Figure 2. The temperature rise required to increase water pressure from hydrostatic to lithostatic (data are from Burnham *et al.* 1969).

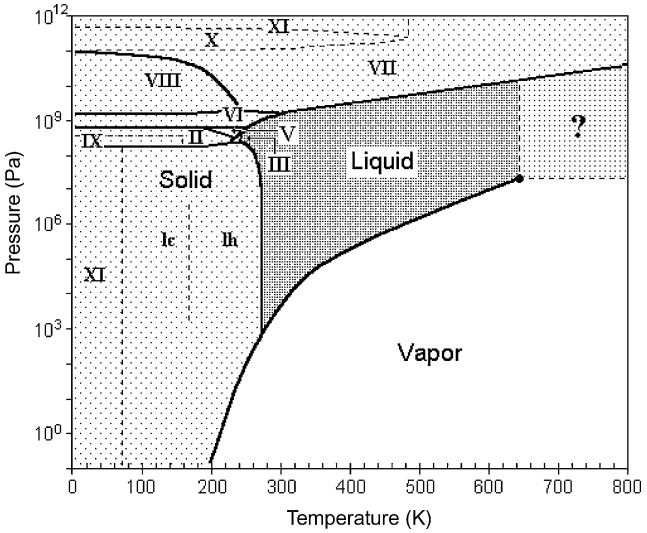

Figure 3. The phase diagram of water. The roman numbers indicate the different structures of ice. (Redrawn from IAPWS Release on the values of temperature, pressure and density of ordinary water substance, 1976 and 1994; http://www.iapws.org/release.htm).

While propagating, the temperature of the heat wave decreases, but this is hardly a problem because thermal energy is abundant compared with the heat necessary to bring water pressure, which is the main pore fluid constituent, from hydrostatic to the lithostatic transition by differential thermal expansion (see Fig. 2; *cf.* also Sibson 1977; Lachenbruch 1980; Mase & Smith 1987). For example, considering a depth of 10 km, a temperature rise of approximately 70 °C produces a pressure increase ~ 0.2 GPa, which is sufficient to decrease friction towards zero in the approximation that dynamic effects can be disregarded. These are essentially granular and viscous resistance effects. The first ones can be traced to transgranular friction induced by dilatancy and are likely to be overcome by a slight fluid overpressure. The second ones are small because sliding velocities should be at most of the order of 1 m s^{-1}.

5.3 Stage III

The stick-slip episode of stage I has generated a frictional heat wave, which in stage II propagates to the whole shear zone inducing a transition of pore pressure from hydrostatic to lithostatic. Once the shear zone has been pressurized, slipping can occur in a completely different way and the process enters stage III. Note that because the grains in the gouge follow a power-law distribution (*cf.* Section 3), slipping will be a threshold process ruled by the largest grains, which have a size comparable to that of the shear zone. In other words, no slip will occur until the whole shear zone is pressurized.

Propagation was stopped at the end of stage I by reaching the boundary of the set Σ on which

$$\sigma = \sigma_f = (\sigma_n - P_p)\phi, \tag{27}$$

with $\phi \simeq 0.6$–0.9. However, the thermalization of the shear zone, which occurred in stage II, has brought the coefficient of friction ϕ to ~ 0, so that σ is largely unbalanced and slip starts again.

The energy function is now

$$\Psi = E_E - \Delta W_T > 0 \tag{28}$$

and, disregarding granular effects and viscous resistance, slip will occur with

$$E_E \simeq E_R \tag{29}$$

virtually radiating all the residual deviatoric elastic energy in seismic waves. In light of this, seismic efficiency is ~ 1. The total accumulated strain, which is of the order of 10^{-3}, is released. On a single patch, the latter corresponds to a slip of 10^{-2} m, which occurs at velocities that seismology allows to estimate as of the order of 1 m s^{-1} (*cf.* Ben-Menahem & Singh 1981), yielding a characteristic time $\sim 10^{-2}$ s.

Note how the assumption upon which stage III is based is that no reduction in the pressure of the shear zone occurs before the radiative slip is completed. This assumption is unfortunately very difficult to verify for experimental reasons: the current knowledge of frictional sliding in fault gouge material at velocities larger than 10^{-2} m s^{-1} is extremely limited even at room pressure (Tsutsumi & Shimamoto 1997; Hammerberg *et al.* 1998; Roder *et al.* 1998, 2000) and at the 10 MPa pressures of the seismic focal regions, when slip velocity increases, high-friction–high-velocity slip possibly occurs at some spots. On the latter, high temperatures are locally attained, which possibly induce a water-vapor transition producing a local abatement in friction, as well as a decrease in temperature as a result of the latent heat of evaporation, preventing the formation of melting products. Data are lacking also in this respect, because the phase diagram of water is virtually unknown in the region above 600 K and 10 MPa (see Fig. 3), in which water is probably in a supercritical phase, with liquid-like hydrogen-bonded clusters dispersed within a gas-like phase. The physical properties of the latter, such as gas- or liquid-like behaviour, are likely to vary abruptly in response to changing density (Hasegawa *et al.* 2003). Another possibility is that a gel is formed (Iler 1979).

5.4 Parallel with the classical single-stage case

All the current earthquake models, including the cellular automata of the complex physics approach (Main 1996; Rundle *et al.* 2000; Mulargia & Geller 2003), assume a single stage. This is similar to our stage I, but has the fast slip of our stage III. To start such a single-stage process on a patch, the value of σ should suddenly jump to a value

$$\sigma \gg \sigma_f \tag{30}$$

to produce a slip large enough to emit significant elastic radiation, because this is proportional to the slip s (*cf.* eq. 9), while our model requires much smaller stress jumps to be ignited. Stress variations in the Earth's crust are related to several factors. The largest changes are caused by tectonic loading, which acts at constant and very low strain rates lower than $\sim 10^{-15}$ s^{-1}. Tidal stresses are periodic with strain rates of 10^{-13} s^{-1} and similar values are attained also by atmospheric loads, albeit with no periodicity (e.g. Ohtake & Narakahara 1999). In addition to these, there is the stress transfer induced by the occurrence of other earthquakes [e.g. the Coulomb failure stress; *cf.* Harris (1998); *cf.* also Section 6.2], which may reach similar strain values, but with shorter insertion times and thus higher rates. Disregarding tectonic load for its constant low rate, stress jumps are thus induced by the superposition of mostly non-periodic functions. The probability of a stress jump $\Delta\sigma$ of energy $E_{\Delta\sigma}$ can therefore be assumed as random and taken to follow a Boltzmann statistic

$$p(E) \propto e^{-(E_{\Delta\sigma}/k_B T)}, \tag{31}$$

or (*cf.* eq. 2)

$$p(\Delta\sigma) \propto e^{-(C^{-1}\Delta\sigma)^2/k_B T}, \tag{32}$$

where C and k_B are respectively the elastic and Boltzmann constants. The last equation suggests that the large jumps required by single-stage models are (square-)exponentially less likely than those required by the three-stage model.

Another possibility is that no large jump occurs, but there exist alternative single-stage processes capable of abating friction. There seem to be two candidates. The first one is a roller bearing effect resulting from generalized rolling processes in the fault gouge grains (*cf.* Mora *et al.* 2000). However, this effect appears at best capable of reducing the friction coefficient ϕ to 0.3 (ibid.), which according to eq. (13) merely implies a factor of ~ 2 reduction in the heat produced, insufficient to accommodate the heat flow paradox.

The other candidate is that local melting, produced by initial sliding, acts as a lubricant for further slip (*cf.* Kanamori & Heaton 2000). There are basic difficulties in applying such a mechanism. First, at the timescale involved by a single-stage process (eq. 26) all thermal processes regard only a thin zone of $<10^{-3}$ m around the sliding plane. Melting can therefore possibly act as a lubricant only on sliding surfaces flat with $<10^{-3}$ m accuracy. While the latter is easily attained on 10 m machined blocks with good industrial equipment, such an accuracy is unthinkable in natural materials, particularly in fault gouge, where the power-law distribution of grain size makes the larger grains, with size $\sim 10^{-2}$ m, control the slipping. Secondly, the presence of melting products (i.e. pseudotachylites) is so scarce in exhumed faults (Magloughlin & Spray 1992; Sibson 1992) that frictional melting appears to be a secondary effect, occurring only locally in a highly fractured and crushed environment, (*cf.* McKenzie & Brune 1972; Sibson 1973; Spray 1987). Some further discussion on this point is given in Section 6.3 below.

This concludes our elementary description relative to a single patch. However, earthquakes are cooperative phenomena and a number of patches will always be involved. We will now therefore discuss the process for a set of patches.

6 EARTHQUAKES AS COOPERATIVE PHENOMENA

Let us first of all analyse the number of patches that cooperatively take part in the slip. If we were to apply strict self-similarity to our basic element (Fig. 1), we would have an earthquake represented by the simultaneous slip of all the patches within the two megacubes of side R with 10 m $\leq R \leq 10^4$ m, where R^2 gives a direct measure of event size. We will rather assume self-similarity as a statistical property so that not all the patches on the domain $R \times R$ slip, but $R \times R$ defines the characteristic size of the slipping domain. Recall also that our assumption of self-similarity, just as any real self-similarity, regards a finite range (*cf.* Section 3). In our case this is limited below by the characteristic length of fault gouge and above from the vertical dimension of the seismogenic crust.

6.1 Earthquake size

Assuming self-similarity as a statistical property, the size of the earthquake is given by the number of patches that undergo together a stage III slip, which are primarily (but not only, see strain transfer in Section 6.3 below) the geometrically connected patches that have simultaneously entered stage I. This means that the size of the event will be determined $\sim 10^2$ s before the start of stage III in which the radiation of elastic waves occurs. The patches simultaneously entering stage I are those for which at the instant $t = t_0$ there is a transition with a stress level just above the friction stress σ_f

$$\sigma_{t<t_0} < \sigma_f \quad \rightarrow \quad \sigma_{t=t_0} > \sigma_f. \tag{33}$$

The occurrence of such a transition over a set of patches as a result of random fluctuations (generally superimposed to a deterministic evolution function) is described in statistical mechanics by the correlation length ℓ, which represents the length over which cooperative effects occur. This length depends on the laws defining the model and its evolution, which are generally based on local threshold processes (as it happens for our single patches) and this leads to strongly non-linear dynamics.

The most simple description of such systems is provided by percolation theory (e.g. Stauffer & Aharony 1994), while more detailed pictures are given by cellular automata (e.g. Burridge & Knopoff 1967; Bak & Tang 1989; Carlson & Langer 1989), which are computer algorithms simulating a lattice of cells ruled by laws describing their interaction and the external forcing. The general result of all such models is that the correlation length is distributed according to an inverse power (e.g. Stauffer & Aharony 1994; Castellaro & Mulargia 2002), so that the probability of an event of given size follows a power law, reproducing the observed distribution for earthquake size, which is known as Gutenberg–Richter law. This behaviour, which is one of the main phenomenological features of earthquakes, can possibly be derived by using simple mean-field arguments (*cf.* Anton 1999). All these approaches concur in that the probability of an event of given size is tied to the probability of having the corresponding correlation length, which follows a negative power law. This happens in all single-stage cellular automata models and also in the three-stage model we propose, with some minor differences related to strain transfer discussed below.

6.2 Global radiative and ignition slips

The second effect produced by the cooperative nature of the process is on global slip.

Relying on statistical self-similarity, we assume that the region involved in the process is defined by the double cubic domain embedding the set of patches that slip (see Fig. 4). The side l of each cube is Ω times the unit patch and is equal to the correlation length ℓ. Consistently with our original self-similarity assumption, we take the maximum strain on such volume as constant and equal to

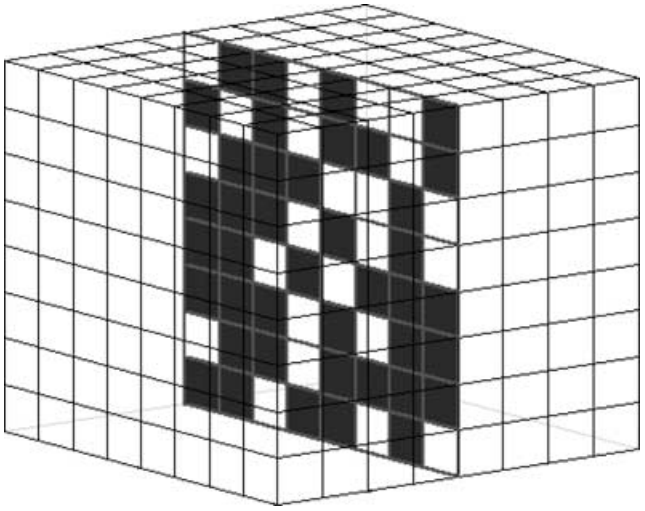

Figure 4. The 3-D square lattice that we assume for a portion of crust containing the seismic fault, which is shown as a 2-D slice. The cells that have slipped in a given event are shown in black. The linear dimension of each cell is ~ 10 m.

$\epsilon \sim 10^{-3}$ so that the global volume involved in the release of elastic energy (see Fig. 1) is $\propto \Omega^3$. According to eq. (3), the global fault slip s that releases this strain is $\propto \Omega$ and the slip surface is $\propto \Omega^2$. The way in which self-similar strain release on the megacubes leads to the addition of local slip contributions in each patch to give the global (average) slip of eq. (3) is pictorially shown in Fig. 5. This yields a global slip of the order of 1 m for $\Omega \sim 10^2$, i.e. for correlation lengths $\sim 10^3$ m. Note how this would imply slip durations of the order of 1 s, during which the pressurization of the shear zone would have to stay at (or above) the lithostatic value.

Which portion of this slip is used for thermalization (from now on we call this the ignition slip) and which for radiation (from now on we call this the radiative slip)? Starting from stage I, we consider that, because the ignition slip is fixed at $\sim 10^{-3}$ m irrespective of correlation length, the strain release required to complete stage I and the following stage II (the ignition strain), is $10^{-4}\Omega^{-1}$. This means that each single patch contributes to the ignition strain proportionally to Ω^{-1}, i.e. spending for ignition a smaller proportion of the accumulated strain, the larger is the domain entering stage I.

This argument makes large events energetically favoured by a factor $\propto \Omega$. However, such events require also on the strain level a correlation length $\propto \Omega$, which has probability

$$p \propto \Omega^{-\beta} \tag{34}$$

with β (*cf.* Stauffer & Aharony 1994) depending on the specific model (for example, for a Bethe lattice $\beta = \frac{5}{2}$). This yields that large events are unfavoured by a factor $\propto \Omega^{1-\beta}$ (for a Bethe lattice $\Omega^{-1.5}$ which incidentally matches the Gutenberg–Richter law, because taking event size $10^m \propto \Omega^2$ requires that m is distributed as $\log\ N = a - bm$, with $b \simeq 1$).

Because the strain release in stage III is $\sim 10^{-3}$, while the strain required for thermalization is $\sim 10^{-4}\Omega^{-1}$, we can define the ratio of ignition strain to the radiative strain as

$$\gamma \simeq 10^{-1}\Omega^{-1}, \tag{35}$$

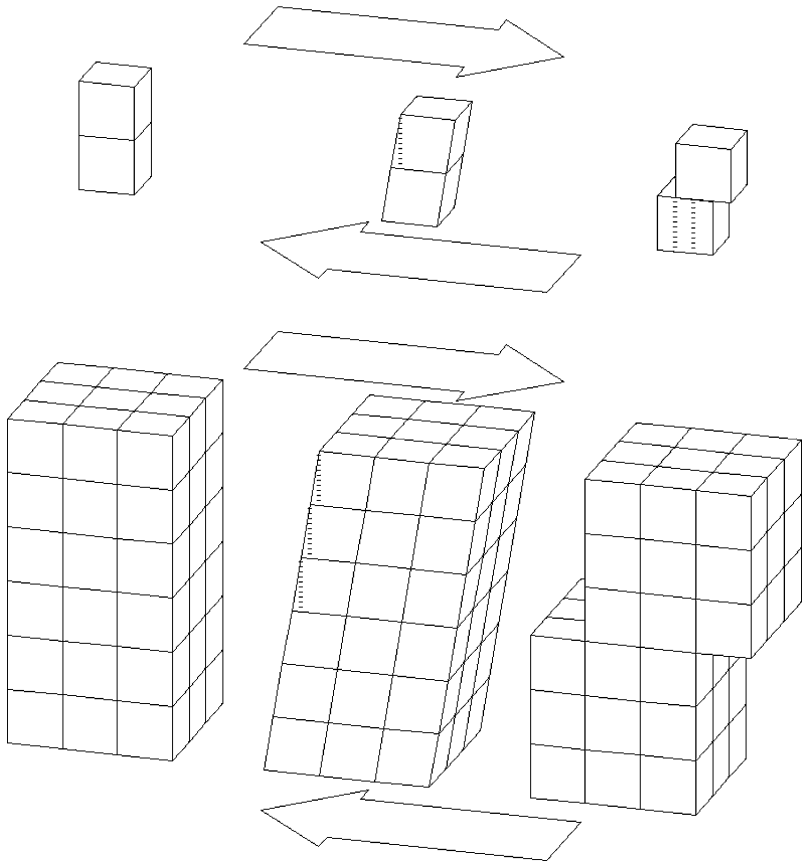

Figure 5. The self-similar way in which a constant and unitary shear strain release at each patch combines to produce global constant slip equal to Ω times that on a single patch, under the assumption that boundary effects are disregarded.

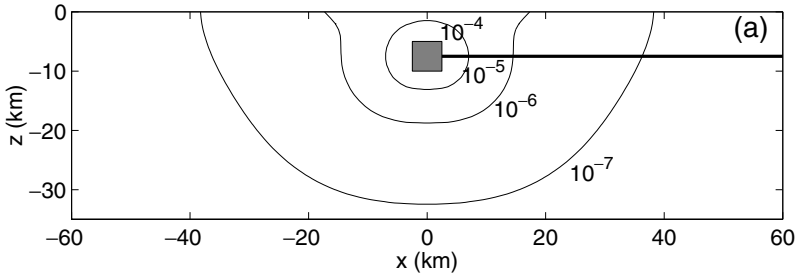

Figure 6. Strain contours on the fault plane for a vertical strike-slip square fault with 5 km side, 5 km depth of the upper rim and slip equal to $\frac{5}{3}$ m according to the formulation of Okada (1992). The line (a) is related to Fig. 7.

so that for any sizable earthquake (i.e. with source size $\geq 10^3$ m) the energy required to start the process is some orders of magnitude smaller than the later elastically radiated energy. The expression $\eta \simeq 1 - \gamma$ is the seismic efficiency of the process, which increases with earthquake size, and is in any case very close to 1, at odds with classical models, where it is of the order of a few 10^{-2} (e.g. Shearer 1999).

Finally, note that the ignition stress of an event with $\Omega \sim 100$–1000, i.e. with a source slip surface of 1×1 to 10×10 km is $\sim 3 \times 10^{-2}$ to 3×10^{-3} MPa. Therefore, the model provides an explanation for the fact that small values of stress transfer may trigger seismic events, an issue that has been long questioned on physical grounds (*cf.* Harris & Simpson 1992; Du & Aydin 1993; Bennett *et al.* 1995; Dodge *et al.* 1995; Astiz *et al.* 2000). The last two results appear capable to reconcile Coulomb failure stress theory with experimental evidence.

6.3 Strain transfer

The third effect produced by the cooperative nature of the process is the strain transfer that an element that slips induces on the neighbouring elements. Let us consider a neighboring patch Λ on which this strain transfer has increased the stress level of $\Delta\sigma$ from the value σ_0 to the value $\sigma_{\text{transf}} = \sigma_0 + \Delta\sigma$. There are three possible cases, considering that the radiated energy is proportional to the slip s (*cf.* eq. 9):

(i) Case A:

$$\sigma_{\text{transf}} < \sigma_f; \tag{36}$$

nothing happens.

(ii) Case B:

$$\sigma_{\text{transf}} \geq \sigma_f; \tag{37}$$

the element Λ exhibits a small slip sufficient to make it enter stage I and after $\sim 10^2$ s it undergoes a stage II–III transition.

(iii) Case C:

$$\sigma_{\text{transf}} \gg \sigma_f; \tag{38}$$

the element Λ exhibits a slip sufficient to make it enter stage I and to continue slipping. If $\Delta\sigma$ is large it may induce a slip s sufficient to emit significant elastic radiation, albeit with high friction, low efficiency and a strong production of heat that should show up in melting products. After $\sim 10^2$ s it undergoes a stage II–III transition releasing the residual strain.

Disregarding the directional effects, cases A, B and C can be expected to correspond approximately to $\Delta\epsilon$ values respectively $10^{-7} \leq \epsilon \leq 10^{-5}$ and $10^{-4} \leq \epsilon$. To estimate the importance of this effect let us analyse a practical example.

Following our self-similar geometry, let us take the slip surface as a dislocation on a square domain and estimate the local change in strain from the (static) elastic solution of Okada (1992). The detail of the spatial distribution of $\Delta\varepsilon$ depends on the specific fault parameters, but the general behaviour is a strong decrease with distance r from the fault (see Fig. 6), which is well approximated by a power law $r^{-\alpha}$ with α between 2 and 3 (*cf.* Cotton 1995). For example, taking a vertical strike-slip square fault with 5 km side, 5 km depth of the upper rim and slip equal to $\frac{5}{3}$ m (the reason for the latter choice will be apparent in next section) and limiting the analysis to the fault plane, yields a value of $\alpha = 2.2$ (see Fig. 7). This stands for a fairly short-range behaviour, with strain transfer perturbations extending over comparatively small areas.

Note how the cascades in all the classical single-stage cellular models are ruled by case C alone. This means that a large event involving the slip of Ω^2 patches requires a correlation length $\propto \Omega$ both in the classic single-stage model and three-stage model we propose. The only difference is that in the model we propose small perturbations are required to induce a case B behaviour, while in the classic case (much less likely) large stress jumps are required to induce a case C behaviour.

6.4 Self-similarity on the fault plane and stress drop

The fourth effect produced by the cooperative nature of the process regards the geometry of the slip on the fault and the stress drop. In the present section, let us for simplicity disregard border effects, so that patches on the fault that are neighbour to non-slipping patches experience no slip reduction.

Geometrically, a fault is a fractal, albeit not too far from a plane (Okubo & Aki 1987), so that it can be roughly approximated as a plane. Let us use this approximation and assume statistical self-similarity for the slipping patches over the fault plane. In statistical mechanical terms this is equivalent to the proximity to a critical state (*cf.* Mulargia & Geller 2003). This also suggests a fractal geometry with fractal dimension close to that of percolation, which is equal to 1.896. To set the discussion in the most simple possible terms, we note that the latter is very similar to the fractal dimension of a square Sierpinski carpet (see Fig. 8), which is equal to 1.893, and we take this geometry as representative of the global slip on the fault surface, disregarding any specific lacunarity problem. Obviously, the fractal geometry has to be intended on a finite scaling range, as is customary for all applications to the real world (e.g. Feder 1988). In other words, geometrical self-similarity occurs over a finite domain, which in our case is limited to approximately 3.5 decades, consistent with the

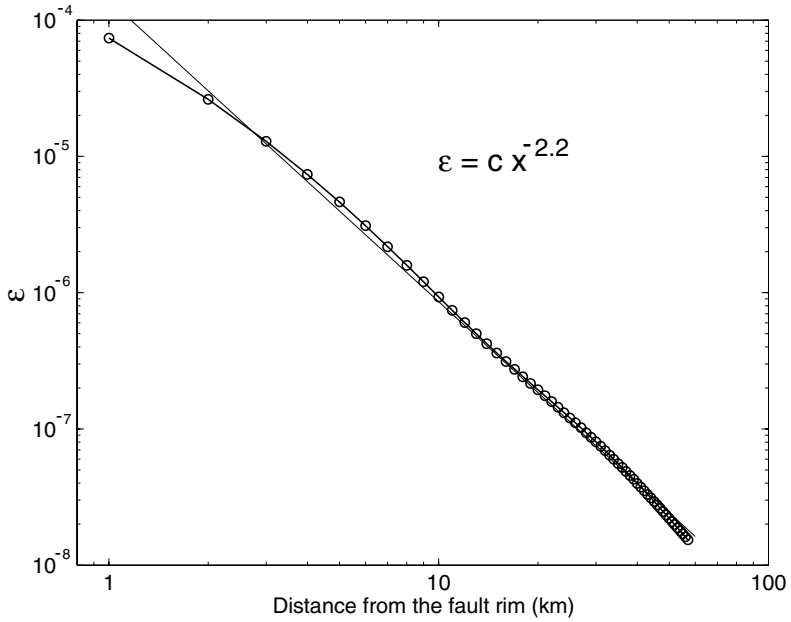

Figure 7. The decay of shear strain with distance from the fault front rim along the line (a) for the fault of Fig. 6. The data are well fitted by a power law with exponent −2.2.

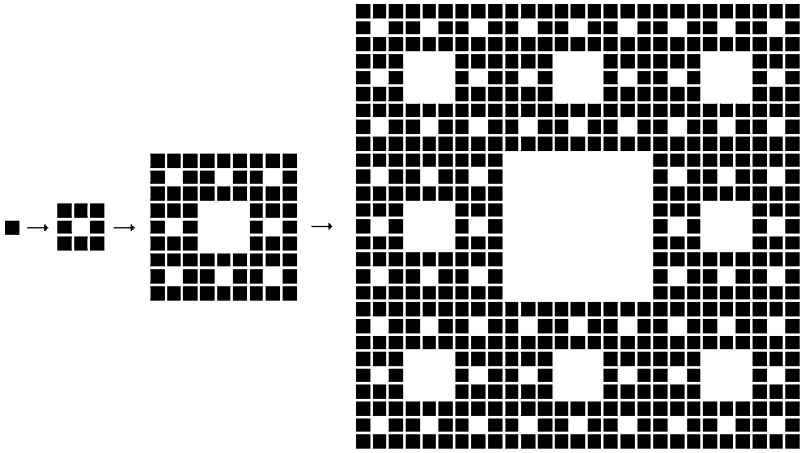

Figure 8. A Sierpinski carpet, which has a fractal dimension very close to that of percolation and can thus be taken as roughly representative of criticality (see text). The slipped patches are in black. Note that at zero order the whole patch seems to slip, as in the seismological model.

definition of our patch (*cf.* eq. 3) as well as with the constraint for a correct fractal attribution (*cf.* Ciccotti & Mulargia 2002).

Assuming that slip occurs on the latter finite range fractal domain (see Fig. 4) rather than on the entire fault surface implies first of all that the total area of the slipped patches is approximately $\frac{2}{5}$ that of the embedding square. As a consequence, the stress drop calculated according to the standard average over the embedding square fault gives a value that is $\sim \frac{2}{5}$ of what really occurs on each patch, making it appear as a partial strain release. Border effects around each slipping patch, which have been disregarded here, are likely to further reduce this fraction. This apparent partial release is an artefact of considering the slip averaged on the square embedding the fractal set of the patches. The fraction of the apparent partial release depends on the self-similarity range and fractal dimension, but not on the embedding fault size. It is therefore independent of event size, in agreement with the apparent stress drop approximate constancy, which seems a well established phenomenological and unexplained empirical result (Abercrombie & Leary 1993). In addition to this, one has to recall that the embedding fault area cannot be accurately constrained by seismological and geodetic measurements and is likely to be overestimated (*cf.* Hardebeck *et al.* 1998), so that the usual average interpretation is likely to imply a further, and possibly large, reduction of the apparent average stress drop.

Following the same reasoning also, the average slip will be apparently reduced by the same factor. In fact, taking an event of seismic moment $M = \mu\, sA$, its value can be reconciled with the usual average over the embedding fault by either reducing the apparent stress drop, as we just did, or the slip s, or by reducing both by the appropriate fraction. Note also how a set of patches of linear dimension 10^2 (with a global length of 10^3 m) following Euclidean geometry would have a total slip of the order 1 m, but following the above reasoning would have an apparent average slip of a few tenths of a metre, in agreement with field data (Purcaru & Berckhemer 1982; Jackson *et al.* 1982). For this reason we choose $s = \frac{5}{3}$ m in our example, Fig. 6.

In summary, the assumption of slip over a finite range that is a fractal rather than Euclidean domain implies that only a fraction of the patches on the fault plane slip and only a fraction of the available stress is released. This fraction depends on the geometry ruling the process alone and not on the event size.

7 VALIDATION

The model we propose is rooted in basic physics, but relies on a number of assumptions. At odds with current seismic source models it agrees with the available phenomenology. However, as any physical model, it is not credible without a strict validation. The latter appears difficult, because it requires casting a stringent null hypothesis on a system that is not directly accessible.

Such a null hypothesis can be hopefully formulated in terms of observing two new effects, which are predicted by the model. The first of them is that stage III should induce slip in the non-slipping patches neighbouring the slipping ones within the main-shock fault (Fig. 4) according to case C above. In the example fault we have worked out, which disregards the fractal nature of the faulting and therefore overestimates the strain field, the induced shear strain on the fault plane is 10^{-4} only immediately outside the fault. The induction of high-friction slip is therefore expected close to the border of the slipping patches, where a stronger concentration of pseudotachylites should be observed.

The second effect is that, because the induced strain is $\sim 10^{-6}$–10^{-7} at distances equal to $\sim$ 3–6 fault lengths, a surge of aftershocks should be observed in a quite large area with a delay of $\sim 10^2$ s from the main shock.

Neither of these effects appears easy to observe. The first one because later-stage deformation and weathering tend to inhibit the detection of pseudotachylytes. The second one because the coda of the main event blurs the seismic records for an interval that has a duration t_e (*cf.* Lee *et al.* 1972; Gasperini 2002)

$$\log t_e \simeq mC_1 + C_2, \tag{39}$$

where m is magnitude and the constants $C_1 \sim \frac{2}{5}$, and $C_2 \sim \frac{4}{5}$, which gives coda durations larger than 10^2 s for events with $m \geq 3$.

8 CONCLUSIONS

Based on the physical arguments of self-similarity, energy balance and scale analysis, we developed an earthquake source model in which energy release occurs in three stages rather than in a single stage and slip occurs over a fractal rather than Euclidean domain, as it happens in all current models. Our model, which has a global radiative efficiency close to unity, seems capable of reconciling the available and apparently contradictory laboratory and *in situ* evidence, including high- and near-zero friction values, lack of heat flow anomaly, aftershock triggering according to Coulomb formulation, self-similar strain release, partial and constant stress drop. On the other hand, it relies on the assumption that the pressurization of the shear zone can be sustained during the radiative slip process, an issue that is experimentally very poorly constrained as a result of the almost total lack of data on high-velocity slip and phase diagram of water above 600 K and 10 MPa. The model lacks in any case a strict validation, which may come from the observation of two additional effects it predicts: a higher concentration of pseudotachylites near the border of slipping patches and a surge of aftershocks in a wide area surrounding the main-shock fault with a $\sim 10^2$ s delay.

ACKNOWLEDGMENT

The authors wish to thank Ian Main and Stefan Hergarten for their constructive reviews.

REFERENCES

Abercrombie, R. & Leary, P., 1993. Source parameters of small earthquakes recorded at 2.5 km depth, *Geophys. Res. Lett.,* **20,** 1511–1514.

Anton L., 1999. Simple equation for earthquake distribution, *Phys. Rev.*, E., **59,** 7213–7215.

Astiz, L., Shearer, P.M. & Agnew, D.C., 2000. Precise relocations and stress change calculations for the upland earthquake sequence in southern California, *J. geophys. Res.,* **105,** 2937–2953.

Bak, P. & Tang, C., 1989. Earthquakes as a self-organized critical phenomenon, *J. geophys. Res.,* **94,** 635–637.

Ben-Menahem, A., 1995. A concise history of mainstream seismology – origins, legacy, and perspectives, *Bull. seism. Soc. Am.,* **85,** 1202–1225.

Ben-Menahem, A. & Singh, S.J.S., 1981. *Seismic waves and sources*, Springer-Verlag, New York.

Bennett, R.A., Reilinger, R.E., Rodi W. & Li, Y., 1995. Coseismic fault slip associated with the 1992 m(W)-6.1 Joshua-Tree, California, earthquake - implications for the Joshua-Tree Landers earthquake sequence, *J. geophys. Res.,* **100,** 6443–6461.

Ben-Zion, Y., 2001. Dynamic ruptures in recent models of earthquake faults, *J. Mech. Phys. Solids,* **49,** 2209–2244.

Brudy, M., Zoback, M.D., Fuchs, K., Rummel, F. & Baumgartner, J., 1997. Estimation of the complete stress tensor to 8 km depth in the KTB scientific drill holes: implications for crustal strength, *J. geophys. Res.,* **102,** 18 453–18 475.

Brune, J.N., 1968. Seismic moment, seismicity, and rate of slip along major fault zones, *J. geophys. Res.,* **73,** 777–784.

Brune, J.N., Henyey, T.L. & Roy, R.F., 1969. Heat flow, stress and rate of slip along the San Andreas Fault, California, *J. geophys. Res.,* **74,** 3821–3827.

Burnham, C.W., Holloway, J.R. & Davis, N.F., 1969. Thermodynamic properties of water to 1000 C and 10,000 bars, *Geol. Soc. Am. Spec. Paper*, Paper 132.

Burridge, R. & Knopoff, L., 1967. Model and theoretical seismicity, *Bull. seism. Soc. Am.,* **57,** 341–371.

Byerlee, J.D., 1978. Friction of rocks, *Pure appl. Geophys.,* **116,** 615–629.

Carlson, J. M. & Langer, J. S., 1989. Properties of earthquakes generated by fault dynamics, *Phys. Rev. Lett.,* **22,** 2632–2635.

Carslaw, H.S. & Jaeger, J.C., 1986. *Conduction of heat in solids*, 2nd edn. Oxford University Press, Oxford.

Castellaro, S. & Mulargia, F., 2002. What criticality in cellular automata models of earthquakes?, *Geophys. J. Int.,* **150,** 483–493.

Ciccotti, M. & Mulargia, F., 2002. Pernicious effect of physical cutoffs in fractal analysis, *Phys. Rev.*, E., **65,** 37 201–37 204.

Clark, S.P., 1966. *Handbook of physical constants*, Geol. Soc. Am. Mem., New York.

Cotton, F., 1995. Imagerie de la source seismique par inversion des mouvements forts et étude des variations de contraintes associés aux seismes, *PhD Thesis,* Joseph Fourier University, Grenoble.

Dahlen, F.A., 1977. The balance of energy in earthquake faulting, *Geophys. J. R. astr. Soc.,* **48,** 239–261.

Dodge, D.A., Beroza, G.C. & Ellsworth, W.L., 1995. Foreshock sequence of the 1992 Landers, California, earthquake and its implications for earthquake nucleation, *J. geophys. Res.,* **100,** 9865–9880.

Du, Y.J. & Aydin, A., 1993. Stress transfer during 3 sequential moderate earthquakes along the central Calaveras fault, California, *J. geophys. Res.,* **98,** 9947–9962.

Eshelby, J.B., 1969. The elastic field of a crack extending nonuniformly under general anti-plane loading, *J. Mech. Phys. Solids,* **17,** 177–199.

Feder, J., 1988. *Fractals*, Plenum Press, New York.

Freund, L.B., 1998. *Dynamic fracture mechanics*, Cambridge University Press, Cambridge.

Gasperini, P., 2002. Local magnitude revaluation for recent Italian earthquakes (1981–1996), *J. Seismol.,* **6,** 503–524.

Geller, R.J., Jackson, D.D., Kagan, Y.Y. & Mulargia, F., 1997a. Earthquakes cannot be predicted, *Science,* **275,** 1616–1617.

Geller, R.J., Jackson, D.D., Kagan, Y.Y. & Mulargia, F., 1997b. Cannot earthquakes be predicted?, *Science,* **278,** 488–490.

Griffith, A.A., 1920. The phenomena of rupture and flow in solids, *Phil. Trans. R. Soc. Lond.*, A., **A221,** 163–198.

Gutenberg, B. & Richter, C.F., 1956. Earthquake magnitude, intensity, energy and acceleration, *Bull. seism. Soc. Am,* **46,** 105–145.

Hammerberg J.E., Holian B.L., Roder J., Bishop A.R. & Zhou S.J., 1998. Non-linear dynamics and the problem of slip at material interfaces, *Phys.*, D., **123,** 330–340.

Hardebeck, J.L., Nazareth, J.J. & Hauksson, E., 1998. The static stress change triggering model: Constraints from two southern California aftershock sequences, *J. geophys. Res.,* **103,** 24 427–24 437.

Harris, R.A., 1998. Introduction to special section: stress triggers, stress shadows and implications for seismic hazard, *J. geophys. Res.,* **103,** 24 347–24 358.

Harris, R.A. & Simpson, R.W., 1992. Changes in static stress on southern California faults after the 1992 Landers earthquake, *Nature,* **360,** 251–254.

Hasegawa, H.H, Li, C.B. & Ohtaki, Y., 2003. Fractional power scaling of excess heat production, *Phys. Lett.*, A., **307,** 222–228.

Herrmann, H.J. & Roux, S., eds, 1990. *Statistical models for the fracture of disordered media*, North-Holland, Amsterdam.

Hirata, T., Satoh, T. & Ito, K., 1987. Fractal structure of spatial distribution of microfracturing in rock, *Geophys. J. R. astr. Soc.,* **90,** 369–374.

Iler, R.K., 1979. *The chemistry of silica*, 866 pp., John Wiley & Sons, New York.

Jackson, J.A., Gagnepain, J., Houseman, G., King, G.C.P., Papadimitriu, P., Soufleris, C. & Virieux, J., 1982. Seismicity, normal faulting and the geomorphological development of the Gulf of Corinth: the Corinth earthquakes of February and March 1981, *Earth planet. Sci. Lett.,* **57,** 377–397.

Kagan, Y.Y. & Jackson, D.D, 1991. Long-term earthquake clustering, *Geophys. J. Int.,* **104,** 117–133.

Kagan, Y.Y. & Knopoff, L., 1980. Spatial distribution of earthquakes: The two-point correlation function, *Geophys. J. R. astr. Soc.,* **62,** 303–320.

Kanamori, H. & Heaton, T.H., 2000. Microscopic and macroscopic physics of earthquakes, in, *Geocomplexity and the Physics of Earthquakes*, pp. 147–164, eds, Rundle, J.B., Turcotte, D.L. & Klein W., AGU Publ., Washington.

Kasahara K., 1981. *Earthquake Mechanics*, Cambridge University Press, Cambridge, pp. 248.

Kostrov, B.V., 1966. Unsteady propagation of longitudinal shear cracks, *J. appl. Math. Mech.,* **30,** 1241–1248.

Lachenbruch, A.H., 1980. Frictional heating, fluid pressure, and the resistance to fault motion, *J. geophys. Res.,* **85,** 6097–6112.

Lachenbruch, A.H. & Sass, J.H., 1980. Heat flow and energetics of the San Andreas fault zone: Magnitude of deviatoric stresses in the Earth's crust and uppermost mantle, *J. geophys. Res.,* **85,** 6185–6222.

Landau, L.D. & Lifshitz, E.M., 1970. *Theory of elasticity*, 2nd edn. Pergamon Press, Oxford.

Lee, W. H. K., Bennet, R.E. & Meagher, K.L., 1972. A method of estimating magnitude of local earthquakes from signal duration, *U.S. Geol. Surv. Open-File Rep. 28*.

Lockner, D.A. & Okubo, P.G., 1983. Measurements of frictional heating in granite, *J. geophys. Res.,* **88,** 4313–4320.

Magloughlin, J.F. & Spray, J.G., 1992. Frictional melting processes and products in geological materials: introduction and discussion, *Tectonophysics,* **204,** 197–206.

Main, I., 1996. Statistical Physics, Seismogenesis and seismic hazard, *Rev. Geophys. Space Phys.,* **34,** 433–462.

Mase, C.W. & Smith, L., 1987. Effect of frictional heating on the thermal, hydrologic and mechanical response of a fault, *J. geophys. Res.,* **92,** 6249–6272.

McGarr, A. & Gay, N.C., 1978. State of stress in the earth's crust, *Ann. Rev. Earth planet. Sci.,* **6,** 405–436.

McKenzie, D. & Brune, J.N., 1972. Melting on Fault Planes During Large Earthquakes, *Geophys. J. R. astr. Soc.,* **29,** 65–78.

Mora, P., Place, D., Abe, S. & Jaumé, S., 2000. Lattice solid simulation of the Physics of fault zones and earthquakes: the model, results, and directions, in, *Geocomplexity and the Physics of Earthquakes*, pp. 105–126, eds, Rundle, J.B., Turcotte, D.L. & Klein W., AGU Publ., Washington.

Morrow, C.A., Shi, L.Q. & Byerlee, J.D., 1981. Permeability and strength of San Andreas fault gouge under high pressure, *Geophys. Res. Lett.,* **8,** 325–328.

Morrow, C.A., Shi, L.Q. & Byerlee, J.D., 1984. Permeability and strength of San Andreas fault gouge under confining pressure and shear stress, *J. geophys. Res.,* **89,** 3193–3200.

Mulargia, F. & Geller, R.J., 2003. *Earthquake Science and Seismic Risk Reduction*, Kluwer Academic Publishers, Dordrecht, pp. 334.

Ohtake, M. & Narakahara, H., 1999. Seasonality of great earthquake occurrence at the northwestern margin of the Philippine Sea plate, *Pure appl. Geophys.,* **155,** 689–700.

Okada, Y., 1992. Internal deformation due to shear and tensile faults in a half-space, *Bull. seism. Soc. Am.,* **82,** 1018–1040.

Okubo, P.G. & Aki, K., 1987. Fractal geometry in the San Andreas fault system, *J. geophys. Res.,* **92,** 345–355.

Ouillon, G., Castaing, C. & Sornette, D., 1996. Hierarchical geometry of faulting, *J. geophys. Res.,* **101,** 5477–5487.

Purcaru, G. & Berckhemer, H., 1982. Quantitative relations of seismic source parameters and a classification of earthquakes, *Tectonophysics,* **84,** 57–73.

Roder, J., Hammerberg J.E., Holian B.L. & Bishop A.R., 1998. Multichain Frenkel-Kontorova model for interfacial slip, *Phys. Rev.*, B., **57,** 2759–2766.

Roder, J., Bishop A.R., Holian B.L., Hammerberg J.E. & Mikulla R.P., 2000. Dry friction: modeling and energy flow, *Phys.*, D., **142,** 306–316.

Rundle, J.B., Turcotte, D.L. & Klein, W., 2000. *Geocomplexity and the Physics of Earthquakes*, AGU Publ., Washington DC.

Sammis, C.G., Osborne, R. Anerson J., Banerdt, M. & White, P., 1986. Self-similar cataclasis in the formation of fault gouge, *Pure appl. Geophys.,* **124,** 53–78.

Scholz C.H., 1990. *The mechanism of earthquakes and faulting*, Cambridge University Press, Cambridge.

Shearer, P., 1999. *Introduction to Seismology*, Cambriudge University Press, Cambridge.

Sibson, R.H., 1973. Interactions between temperature and pore fluid pressure during earthquake faulting—a mechanism for partial or total stress relief, *Nature, Phys. Sci.,* **243,** 66–68

Sibson, R.H., 1975. Generation of pseuodtachylyte by ancient seismic faulting, *Geophys. J. R. astr. Soc.,* **43,** 775–794.

Sibson, R.H., 1977. Kinetic shear resistance, fluid pressures and radiation efficiency, *Pure appl. Geophys.,* **115,** 387–400.

Sibson, R.H., 1992. Power dissipation and stress levels during seismic faulting, *J. geophys. Res.,* **85,** 6239–6247.

Spray, J.G., 1987. Artificial generation of pseudotachylyte using friction welding apparatus: simulation of melting on a fault plane, *J. Struct. Geol.,* **9,** 49–60.

Stauffer, D. & Aharony, A., 1994. *Introduction to percolation theory*, 2nd edn. Taylor & Francis, Philadelphia.

Tsutsumi, A. & Shimamoto, T., 1997. High-velocity frictional properties of gabbro, *Geophys. Res. Lett.,* **24,** 699–702.

Yoshioka, N., 1986. Fracture energy and the variation of gouge and surface roughness during frictional sliding of rocks, *J. Phys. Earth,* **34,** 335–355.

Zhang, S.Q. & Tullis, T.E., 1998. The effect of fault slip on permeability and permeability anisotropy in quartz gouge, *Tectonophysics,* **295,** 41–52.